catalysts

Article

Enhancing Photocatalytic Hydrogen Evolution with Oxygen Vacancy-Modified P/Ag/Ag_2O/Ag_3PO_4/TiO_2 by Using Optimized $NaBH_4$ Reduction Strategy

Xiang Sun [1], Yunxin Zhu [2], Guangqi An [1], Guoping Chen [3] and Yingnan Yang [1,*]

[1] Graduate School of Life and Environmental Science, University of Tsukuba, 1-1-1 Tennodai, Tsukuba 305-8577, Ibaraki, Japan; sunxiang19910304@gmail.com (X.S.)
[2] Faculty of Bioenvironmental Sciences, Kyoto University of Advanced Science, 1-1 Sogabecho Nanjo Otani, Kameoka 621-8555, Kyoto, Japan; zhuyunxin1994@gmail.com
[3] Research Center for Macromolecules and Biomaterials, National Institute for Materials Science, 1-1 Namiki, Tsukuba 305-0044, Ibaraki, Japan
* Correspondence: yo.innan.fu@u.tsukuba.ac.jp; Tel.: +81-29-8534650

Abstract: The introduction of oxygen vacancies (OVs) is a promising strategy to enhance the hydrogen (H_2) evolution efficiency of photocatalysts. Sodium borohydride ($NaBH_4$) is widely used as a reducing agent to introduce OVs, particularly in composite materials. However, its impact on H_2 evolution remains underexplored. In this study, by employing various mass ratios of $NaBH_4$ to P/Ag/Ag_2O/Ag_3PO_4/TiO_2 (PAgT), OVs modified PAgT (R-PAgT) composites, which were synthesized and systematically characterized by XRD, FT-IR, and XPS. R-PAgT-10 with an optimal mass ratio exhibited a superior H_2 evolution efficiency and stability, maintaining its performance over 20 cycles under visible light irradiation, while the higher mass ratio of $NaBH_4$/PAgT led to the disruption of the crystal structure with excessive OVs amounts, resulting in poor stability. This study highlighted the importance of utilizing the optimal mass ratio of $NaBH_4$ to prepare OVs-PAgT for successful and stable H_2 evolution under visible light irradiation, which holds promise for developing efficient and durable photocatalysts for renewable energy applications.

Keywords: P/Ag/Ag_2O/Ag_3PO_4/TiO_2; oxygen vacancy modification; $NaBH_4$ reduction method; optimal mass ratio of $NaBH_4$/PAgT; solar light driven hydrogen evolution

Academic Editors: Guangzhao Wang and Yanbo Li

Received: 15 January 2025
Revised: 3 February 2025
Accepted: 10 February 2025
Published: 11 February 2025

Citation: Sun, X.; Zhu, Y.; An, G.; Chen, G.; Yang, Y. Enhancing Photocatalytic Hydrogen Evolution with Oxygen Vacancy-Modified P/Ag/Ag_2O/Ag_3PO_4/TiO_2 by Using Optimized $NaBH_4$ Reduction Strategy. *Catalysts* **2025**, *15*, 167. https://doi.org/10.3390/catal15020167

1. Introduction

Global reliance on fossil fuels has led to critical issues, including energy crises and environmental pollution [1]. As a response to these challenges, the utilization of eco-friendly hydrogen (H_2) as a clean energy source has emerged as a promising approach for sustainable development and environmental protection [2,3]. In 1972, Fujishima introduced the concept of H_2 production through a photocatalytic water splitting process using titanium dioxide (TiO_2) [4], sparking growing interest due to its eco-friendly potential [5]. However, pure TiO_2 has limitations, such as the limited utilization of visible light and low charge transfer efficiency, which impede its practical application [6–8]. To address these limitations, our laboratory previously developed a novel solar light-driven composite, denoted as P/Ag/Ag_2O/Ag_3PO_4/TiO_2 (PAgT) [9]. In contrast to pure TiO_2, the PAgT composite demonstrated the enhanced utilization of visible light and accelerated electron

separation/transformation rates, resulting in the excellent H_2 evolution under simulated solar light irradiation (the schematic diagram of PAgT is shown in Figure S1).

Furthermore, oxygen vacancy (OV) modification has been recognized as a promising strategy to further enhance photocatalytic activity. Bad'ura and co-authors reported that spin defects modified TiO_2 nanosystems, which exhibited a 1.5-times higher H_2 evolution rate than the original [10]. Moreover, Xu et al. also confirmed that OVs could efficiently improve the H_2 generation ability of TiO_2 under visible light irradiation [11].

OVs have the potential to enhance solar light utilization efficiency and accelerate the separation and transfer of electron–hole pairs in the host photocatalyst [12]. However, it is crucial to note that the quantity of OVs plays a significant role in enhancing the photocatalytic activity of modified catalysts. An insufficient number of OVs may not improve performance efficiently, while an excess of OVs can become recombination centers for electron–hole pairs, ultimately reducing the activity [13]. Therefore, it is paramount to introduce an optimal amount of OVs in the PAgT composite using a suitable method.

Among various methods, the chemical reduction method employing $NaBH_4$ as the reducing agent has been recognized as an attractive approach to introducing OVs into the host photocatalyst [14]. In this method, the cost-effective and easy-to-handle $NaBH_4$ serves as the reducing agent, generating active hydrogen atoms. These active hydrogen atoms subsequently react with oxygen atoms to create water and OVs. The quantity of active hydrogen atoms is positively correlated with the mass ratio of photocatalyst to $NaBH_4$, with a larger ratio leading to the release of a greater number of active hydrogen atoms and a higher concentration of oxygen vacancies in the host photocatalyst. Hence, it is essential to explore the ideal mass ratio of PAgT to $NaBH_4$ for the successful synthesis of the optimal OV ratio in the PAgT composite.

In this study, OV-modified PAgT composites using the chemical reduction method with $NaBH_4$ as the reducing agent were prepared. To investigate the impact on H_2 evolution, the different mass ratios of PAgT to $NaBH_4$ for OVs modification were employed. The H_2 evolution efficiency of the obtained catalysts was assessed under solar light irradiation and their stability was examined through cyclic experiments. Furthermore, comprehensive characterization using XRD, FT-IR, and XPS were conducted to evaluate the crystal structure and elemental composition of the different R-PagT photocatalysts. Based on these results, the potential effect of varying mass ratios of PAgT to $NaBH_4$ on the photocatalytic properties of the composite was proposed.

2. Results and Discussion

2.1. Photocatalytic H_2 Evolution Rate and Stability of R-PAgT Photocatalysts

2.1.1. First Cycle H_2 Evolution Rate of R-PAgT Photocatalysts

The H_2 evolution efficiencies of the R-PAgT catalysts were evaluated under simulated solar light irradiation using methanol as a hole-scavenger. As shown in Figure 1, the mass ratio of PAgT to $NaBH_4$ significantly influenced the H_2 evolution efficiency. It was evident that the rate of H_2 generation experienced a notable increase when the mass ratios of PAgT to $NaBH_4$ were 3:1 and 5:1. Specifically, the H_2 evolution rates for R-PAgT-3:1 and R-PAgT-5:1 were 1607 and 3347 $\mu mol \cdot g^{-1} \cdot h^{-1}$, respectively. These rates were approximately 3.25 and 6.78 times higher than that of pure PAgT (493 $\mu mol \cdot g^{-1} \cdot h^{-1}$). When the mass ratio of PAgT to $NaBH_4$ further increased to 7:1 and 10:1, it had a relatively modest positive impact on the H_2 evolution rate of the prepared catalysts. The H_2 evolution rates of R-PAgT-7:1 and R-PAgT-10:1 were 1027 and 917 $\mu mol \cdot g^{-1} \cdot h^{-1}$, respectively, which were approximately 2.08 and 1.86 times to pure PAgT. However, regarding the mass ratio of 15:1 for PAgT to $NaBH_4$, there was a detrimental effect on the H_2 generation rate of R-PAgT-

15:1, at only about 337 μmol·g^{-1}·h^{-1}, which was significantly lower than original PAgT composite.

These aforementioned results demonstrated that R-PAgT-3:1, R-PAgT-5:1, R-PAgT-7:1, and R-PAgT-10:1 possessed a better H_2 evolution rate than pure PAgT. However, the practical application of photocatalysts heavily relies on their stability and durability. A key factor in this regard is their ability to maintain consistent performance in the long term. Hence, cyclic experiments were carried out on these four photocatalysts to assess their durability and stability.

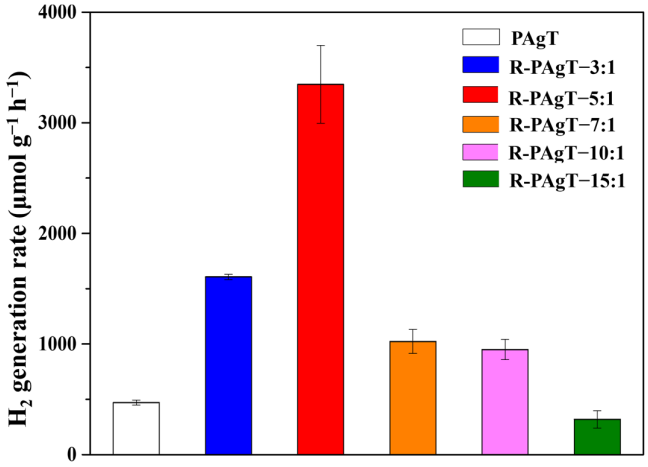

Figure 1. H_2 evolution capability of pure PAgT and R-PAgT under simulated solar light.

2.1.2. Cyclic Experiment of R-PAgT Photocatalysts

The cyclic experiment involving R-PAgT-5:1 was depicted in Figure 2a. In the initial cycle, R-PAgT-5:1 achieved an impressive H_2 evolution rate of 3347 μmol·g^{-1}·h^{-1}. However, this value experienced a decline in the second cycle, dropping to 431 μmol·g^{-1}·h^{-1} and further decreasing to 392 and 368 μmol·g^{-1}·h^{-1} in the third and fourth cycles, respectively. The decline rate of R-PAgT-5:1 was about 89.1%, suggesting its limited stability for practical applications.

In Figure 2b, the cyclic experiment for R-PAgT-3:1 revealed a noticeable trend of decreasing H_2 evolution rate, akin to what was observed for R-PAgT-5:1. During the initial cycle, R-PAgT-3:1 generated approximately 1607 μmol·g^{-1}·h^{-1} of H_2. However, after a single cycle, the H_2 evolution rate of R-PAgT-3:1 showed a steep decline, plummeting to 233 μmol·g^{-1}·h^{-1}, representing a significant 86.2% decrease. This decline strongly suggested that R-PAgT-3:1 exhibited poor stability when considered for practical application. In summary, although R-PAgT-5:1 and R-PAgT-3:1 initially demonstrated excellent H_2 yields in the first cycle, their substantial decline in performance during the second cycle indicated their inadequate stability for practical applications.

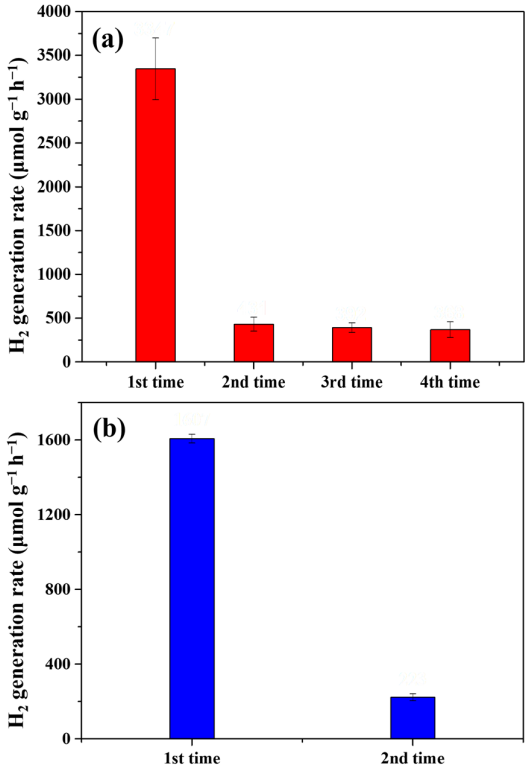

Figure 2. Cyclic experiment for H_2 evolution of (**a**) R-PAgT-5:1 and (**b**) R-PAgT-3:1 under simulated solar light.

The results of the cyclic experiment using R-PAgT-7:1 as a photocatalyst are displayed in Figure 3a. It can clearly be observed that the H_2 evolution rate of R-PAgT-7:1 gradually decreased over the extended number of cycles compared with R-PAgT-5:1 and R-PAgT-3:1. The H_2 evolution rate decreased from 1024 μmol·g^{-1}·h^{-1} in the first cycle to 900 μmol·g^{-1}·h^{-1} in the second cycle. With further extended cycles, i.e., the third to the seventh cycle, the H_2 evolution efficiency slowly decreased to 740, 654, 556, 489, and 450 μmol·g^{-1}·h^{-1}, respectively. The H_2 evolution rate of R-PAgT-7:1 after seven cycles was higher than that of pure PAgT. After that, however, it sharply reduced to 260, and finally reached 158 μmol·g^{-1}·h^{-1} in eighth and ninth cycles, respectively, which was lower than that of pure PAgT (493 μmol·g^{-1}·h^{-1}).

The stability results of R-PAgT-10:1 are displayed in Figure 3b. From the initial cycle to the fifth cycle, the H_2 evolution rates of R-PAgT-10:1 were 903, 823, 712, 602, and 563 μmol·g^{-1}·h^{-1}, respectively, exhibiting a gradual downward trend, which was similar to R-PAgT-7:1. However, in comparison to R-PAgT-5:1, R-PAgT-3:1, and R-PAgT-7:1, R-PAgT-10:1 was able to maintain its H_2 evolution rate at about 632 μmol·g^{-1}·h^{-1} after 20 cycles, which indicated it good stability for practical applications.

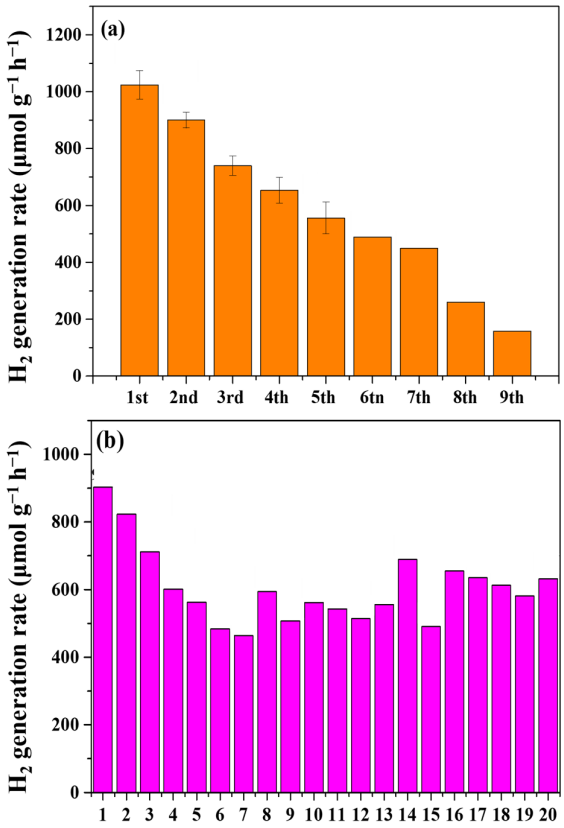

Figure 3. H_2 evolution capability in (**a**) R-PAgT-7:1 and (**b**) R-PAgT-10:1 under simulated solar light.

Based on the above results, it can be summarized that R-PAgT-3:1 and R-PAgT-5:1 exhibited excellent H_2 evolution rates in the initial cycle, but experienced a dramatic decline in the second cycle, which suggests poor stability. It is noteworthy that R-PAgT-10:1 showed a superior H_2 evolution rate compared with pure PAgT, which was a result of the introduction of optimized OVs. Moreover, R-PAgT-10:1 was able to maintain a stable H_2 yield at about 632 μmol·g^{-1}·h^{-1} after 20 cycles, which was much higher the related OV-modified TiO_2 reported (Table S1). In summary, the excellent and stable H_2 evolution performance of R-PAgT-10:1 suggested its potential for practical applications.

2.2. Characterization of R-PAgT Photocatalysts

2.2.1. Crystal Structures of R-PAgT Photocatalysts

The crystal structures of R-PAgT photocatalysts were analyzed through XRD to explain the results of the cyclic H_2 evolution experiments conducted for each photocatalyst. In Figure 4, the pure PAgT composite displayed two distinct diffraction peaks at around 25.4, 37.8, 48.0, 55.1, 62.7, 68.8, and 75.0 degrees, corresponding to the (101), (004), (200), (211), (204), (116), and (215) planes of the anatase TiO_2 phase (JCPDS # 21-1272), respectively [15]. Similarly, both R-PAgT-10:1 and R-PAgT-7:1 exhibited identical diffraction peak positions, indicating that they retained the same anatase TiO_2 phase as the original PAgT composite. This observation suggests that the low mass ratio of PAgT to $NaBH_4$ had minimal impact on the crystal structure of the resulting catalysts. In contrast, the XRD patterns of R-PAgT-5:1 and R-PAgT-3:1 displayed irregular line shapes, with the diffraction peaks of the anatase TiO_2 phase barely detectable in these two catalysts. This anomaly pointed to a significant alteration in the crystal structure of R-PAgT-5:1 and R-PAgT-3:1, likely resulting from an excessive ratio of PAgT to $NaBH_4$. On the other hand, the

characteristic peaks of Ag species were hardly detectable in all the synthesized catalysts, likely due to their low concentrations in the fabrication process.

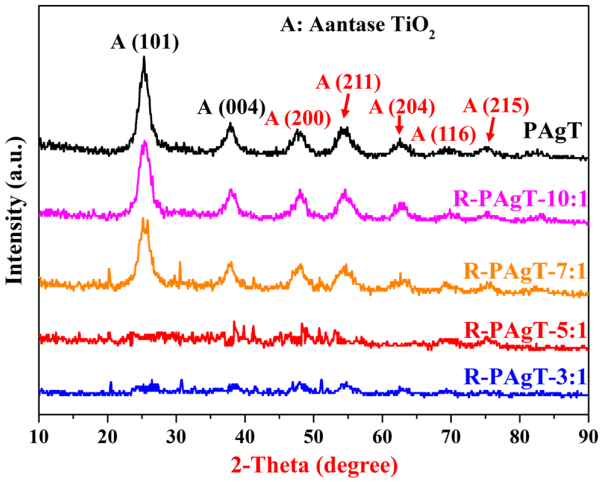

Figure 4. XRD patterns of PAgT and R-PAgT photocatalysts.

2.2.2. Chemical Bonds of R-PAgT Photocatalysts

Moreover, the chemical bonds of R-PAgT were measured using the FT-IR spectrum. As shown in Figure 5, R-PAgT-7:1 and R-PAgT-10:1 processed similar peaks at 3000–3750, 1626, and 400–700 cm^{-1}. The peaks at 3000–3750 and 1626 cm^{-1} were related to the hydroxyl group and surface absorbed water, respectively [16,17]. Notably, the absorption band within 400–700 cm^{-1} is associated with Ti–O stretching vibrations in the anatase TiO_2 lattice [16], indicating the retention of the TiO_2 phase in these two samples. This observation aligns well with the XRD results, further confirming the structural integrity of the TiO_2 component.

In contrast, for R-PAgT-3:1 and R-PAgT-5:1, the characteristic peak in the 400–700 cm^{-1} range was either significantly weakened or nearly absent. This suggests that the TiO_2 structure was disrupted due to the excessive addition of $NaBH_4$ during the synthesis process, leading to the destruction or significant alteration of the TiO_2 lattice. These findings highlight the crucial role of $NaBH_4$ concentration in preserving the TiO_2 framework and emphasize the necessity of optimizing reaction conditions to maintain the structural and functional integrity of the composite material.

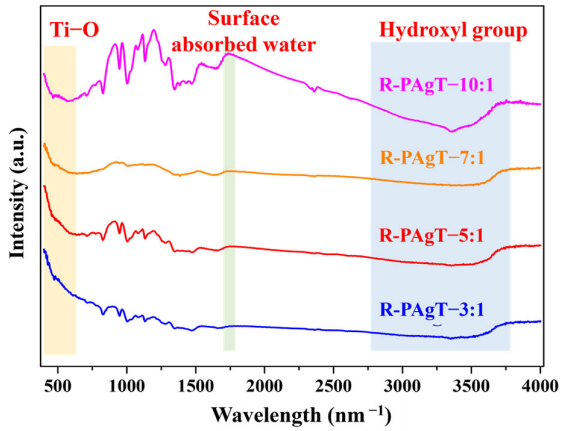

Figure 5. FT-IR spectra of R-PAgT photocatalysts.

2.2.3. Elemental Composition of R-PAgT Photocatalysts

Furthermore, a detailed XPS analysis was performed to determine the elemental composition of R-PAgT catalysts. As depicted in Figure 6, the peaks corresponding to O, Ti, Ag, and P are clearly evidenced in both the pure PAgT and R-PAgT-7:1 and R-PAgT-10:1 sample. This observation suggested that R-PAgT-7:1 and R-PAgT-10:1 maintained the same elemental composition as pure PAgT. In contrast, the peaks for the Ti, Ag, and P elements were conspicuously absent in the XPS spectra of R-PAgT-5:1 and R-PAgT-3:1. This disparity between the small mass ratio (10:1 and 7:1) and the large mass ratio (5:1 and 3:1) of PAgT to $NaBH_4$ underscores the fact that the larger mass ratio had a detrimental effect on the elemental composition of the synthesized catalysts.

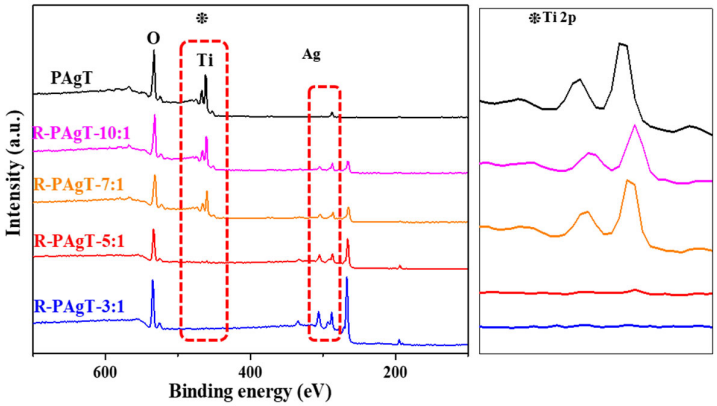

Figure 6. XPS survey spectra of PAgT and R-PAgT catalysts.

The high-resolution Ti 2p XPS spectra of the R-PAgT catalysts are presented in Figure 7. Notably, in the pure PAgT sample, the Ti species displayed two distinct peaks at 458.7 and 464.4 eV. These peaks were attributed to the presence of Ti^{4+} within the TiO_2 component in PAgT composite. Following the chemical reduction process, the Ti 2p XPS spectra of the R-PAgT catalysts exhibited significant alterations. In the case of R-PAgT-7:1 and R-PAgT-10:1, the Ti species could be discerned as four distinct peaks. The peaks at 458.7 and 464.4 eV were associated with Ti^{4+}, while the peaks at 463.2 and 457.8 eV indicated Ti^{3+} [18,19]. The presence of Ti^{3+} confirmed the existence of OVs in R-PAgT [20]. However, when compared to R-PAgT-7:1 and R-PAgT-10:1, the Ti species in R-PAgT-5:1 and R-PAgT-3:1 were primarily centered at 463.2 and 457.8 eV, indicating the presence of Ti^{3+} and OVs in these two catalysts. Notably, in R-PAgT-3:1 and R-PAgT-5:1, no peaks attributed to Ti^{4+} (458.7 and 464.4 eV) were observed. This observation suggests that the use of NaBH4 as a reducing agent during the chemical reduction process could introduce OVs into the PAgT composite. Nonetheless, a higher mass ratio of PAgT to $NaBH_4$ led to the conversion of all Ti^{4+} into Ti^{3+} and an excess of OVs in R-PAgT-3:1 and R-PAgT-5:1.

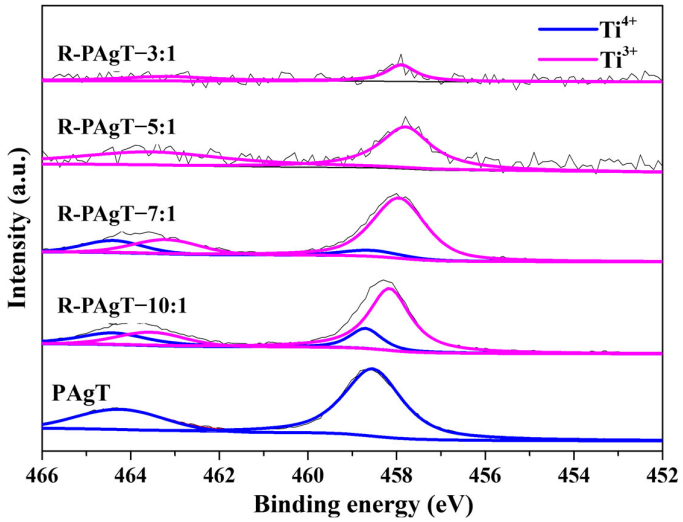

Figure 7. The Ti 2p XPS high-resolution spectra of PAgT and R-PAgT catalysts.

Furthermore, the high-resolution O 1s XPS spectra of the synthesized catalysts are depicted in Figure 8. Evidently, the O species in pure PAgT, R-PAgT-10:1, and R-PAgT-7:1 displayed four discernible peaks. The peak at 529 eV was attributed to Ag–O, indicating the presence of Ag2O within the resulting catalysts [21]. Another peak at 531.3 eV originated from Ti–O–P, signifying the incorporation of phosphorus into the lattice of TiO_2. The peaks situated at 529.7 and 530.9 eV were contributed to lattice oxygen (Ti-O) and non-lattice oxygen (Ti-OH), respectively [21,22]. However, the O species in R-PAgT-5:1 and R-PAgT-3:1 could only be fitted into two peaks, specifically at 530.9 eV (corresponding to the Ti–OH bond) and 531.3 eV (attributed to the Ti–O–P bond). The disappearance of Ag–O and Ti–O bonds in R-PAgT-5:1 and R-PAgT-3:1 strongly indicates that the TiO_2 and Ag_2O components were significantly disrupted due to their reactions with excessive $NaBH_4$. Specifically, $NaBH_4$ served as a strong reducing agent, leading to the reduction in monovalent silver (Ag^+) in Ag_2O to metallic silver (Ag^0), thereby breaking the Ag–O bonds (further corroborated in Figure 9). Simultaneously, the TiO_2 lattice was also affected, likely through partial reduction or structural degradation, resulting in the loss of the characteristic Ti–O vibrational bands. These structural modifications suggest that an excessive $NaBH_4$ ratio during synthesis induces substantial compositional changes.

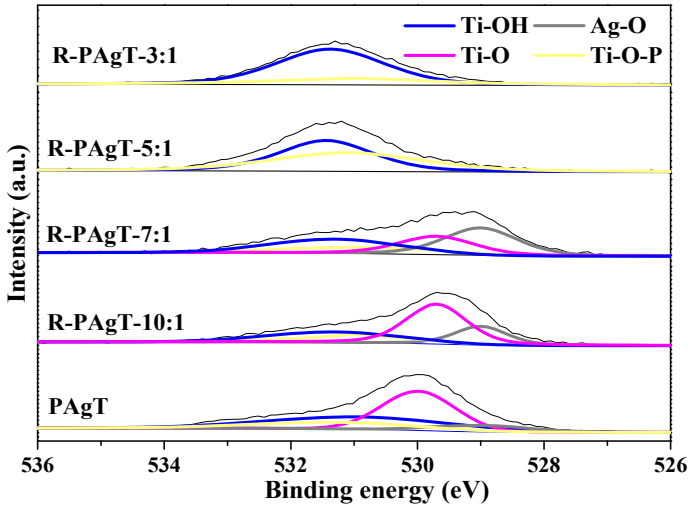

Figure 8. The O 1s XPS high-resolution spectra of PAgT and R-PAgT catalysts.

Additionally, the high-resolution Ag 3d XPS spectra for all the catalysts are presented in Figure 10. In the case of pure PAgT, the peaks at 374.2 and 368.2 eV were associated with metallic Ag^0 [23], while the peaks at 373.4 and 367.4 eV corresponded to Ag^+ ions presented in Ag_2O and Ag_3PO_4, respectively [15]. Following the reduction process with $NaBH_4$, the changes in Ag species in R-PAgT catalysts exhibited a pattern similar to that of the P species. When a small mass ratio of PAgT to $NaBH_4$ was used, the Ag 3d XPS spectra of R-PAgT-10:1 and R-PAgT-7:1 displayed the same four peaks as those in pure PAgT, located at 374.2, 368.2, 373.4, and 367.4 eV. The first two peaks indicated the presence of metallic Ag^0, while the latter two peaks suggested the presence of Ag+ ions in Ag_2O and Ag_3PO_4. However, when compared to R-PAgT-10:1 and R-PAgT-7:1, the Ag 3d XPS spectra of R-PAgT-5:1 and R-PAgT-3:1 could only be fitted to two peaks at 374.2 and 368.2 eV, indicating the presence of metallic Ag^0 in R-PAgT-5:1 and R-PAgT-3:1. These findings suggested that Ag^+ ions in Ag_2O and Ag_3PO_4 were reduced to metallic Ag^0, further indicating the destruction of the Ag_2O and Ag_3PO_4 components when a larger mass ratio of PAgT to $NaBH_4$ was employed.

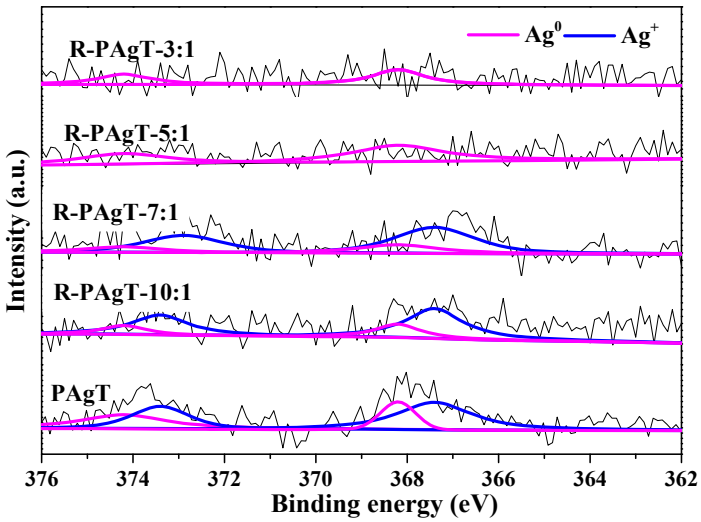

Figure 9. The Ag 3d XPS high-resolution spectra of PAgT and R-PAgT catalysts.

The high-resolution P 2p XPS spectra of the as-synthesized catalysts are illustrated in Figure 10. It is evident that the P species in these catalysts displayed distinct behaviors depending on the mass ratio of PAgT to $NaBH_4$ used during the synthesis process. When a small mass ratio of PAgT to NaBH4 was employed, the P 2p XPS spectra of R-PAgT-10:1 and R-PAgT-7:1 exhibited a single peak at 133.2 eV, which corresponded to the presence of P^{5+} in Ag_3PO_4 [24]. However, in the case of a larger mass ratio of PAgT to $NaBH_4$, it was difficult to fit the P 2p XPS spectra of R-PAgT-5:1 and R-PAgT-3:1 to any P species, indicating the disruption of the Ag_3PO_4 component when a greater ratio of PAgT to $NaBH_4$ was employed.

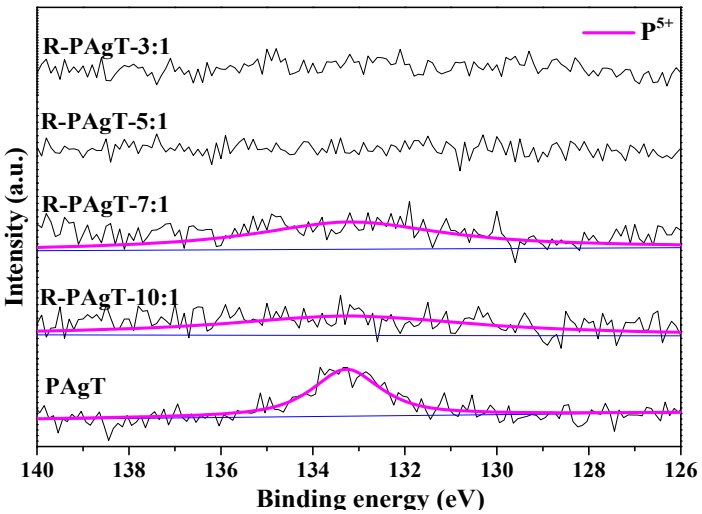

Figure 10. The P 2p XPS high-resolution spectra of PAgT and R-PAgT catalysts.

In summary, the XRD and XPS results presented above highlight the substantial impact of the mass ratio of PAgT to $NaBH_4$ on both the crystal structure and elemental composition of the resulting catalysts. Specifically, R-PAgT-5:1 and R-PAgT-3:1 exhibited compromised crystal structures and an excessive presence of OVs, leading to diminished stability during cyclic experiments. In contrast, R-PAgT-7:1 and R-PAgT-10:1 maintained the same crystal structure and elemental composition as pure PAgT. Furthermore, the presence of Ti^{3+} in R-PAgT-7:1 and R-PAgT-10:1 indicated the successful introduction of OVs into these two catalysts, contributing to the enhanced H_2 evolution rate observed for these samples. Moreover, the relatively robust stability of R-PAgT-10:1 during cyclic experiments can be attributed to the appropriate amount of OVs in this catalyst.

2.3. Different Performances of R-PAgT-7:1 and R-PAgT-10:1

The cyclic experiments conducted with R-PAgT-7:1 and R-PAgT-10:1 revealed that the H_2 evolution rate of R-PAgT-7:1 gradually decreased with extended cyclic time, ultimately falling below that of pure PAgT. In contrast, R-PAgT-10:1 exhibited a different behavior. Remarkably, even after 20 cycles, its performance still outperformed the original PAgT. To elucidate the reasons behind these observations, a comprehensive XRD and XPS analysis was conducted both before and after the use of R-PAgT-7:1 and R-PAgT-10:1, respectively.

As depicted in Figure 11a, after nine cycles, the sample exhibited a lack of discernible peaks around 25.4 and 37.8 degrees, which were attributed to the (101) and (004) planes of the anatase TiO_2 phase. This observation strongly suggested that the crystal structure was compromised, and this occurred after only nine cycles. Furthermore, the chemical state of elements Ti, Ag, O, and P in the post-use R-PAgT-7:1 sample was illustrated in Figure 11b–e. It was apparent that the Ti^{4+} and Ag^{+} species presented in pure R-PAgT-7:1 were reduced to Ti^{3+} and Ag^0 in the sample after nine cycles. Additionally, the presence of Ti-O and Ag-O species, indicative of TiO_2 and Ag_2O, was hardly observable in the sample after nine cycles. These findings strongly suggested that the TiO_2 and Ag_2O components were compromised in the used R-PAgT-7:1. Moreover, the absence of detectable P^{5+} peaks related to Ag_3PO_4 in the used R-PAgT-7:1 further supported the conclusion that its structure was disrupted. In summary, the results from XRD and XPS analyses collectively demonstrated the poor stability of R-PAgT-7:1, rendering it unsuitable for sustained H_2 evolution over an extended period.

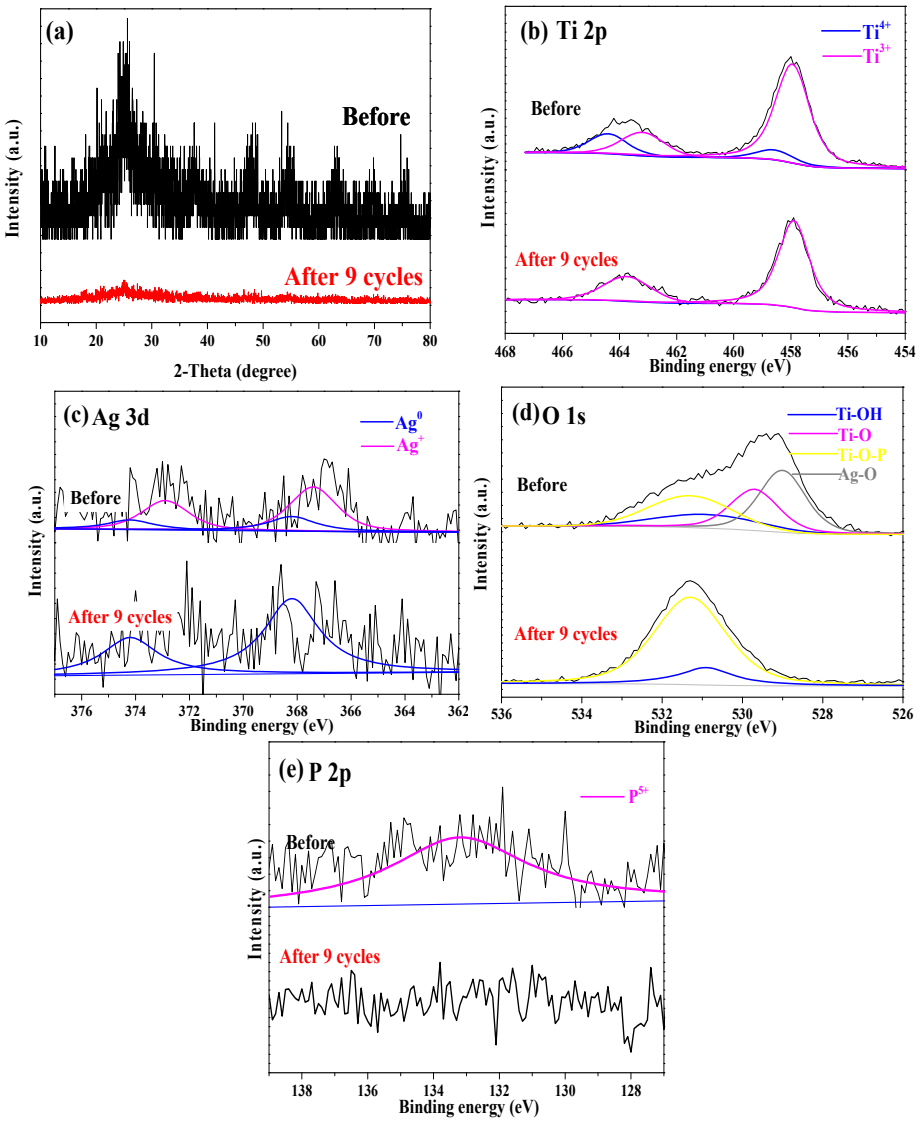

Figure 11. (**a**) XRD patterns, (**b**) Ti 2p, (**c**) Ag 3d, (**d**) O 1s, and (**e**) high-resolution P 2p XPS, before and after the ninth cycle for R-PAgT-7:1.

The XRD patterns for R-PAgT-10:1, both before and after 20 cycles, were presented in Figure 12a. In contrast to R-PAgT-7:1, even after 20 cycles, the peaks corresponding to the (101) and (004) planes of the anatase TiO_2 phase remain distinctly visible in the used R-PAgT-10:1 sample. This observation strongly suggested that the crystal structure of R-PAgT-10:1 remained intact even after 20 cycles. Furthermore, the high-resolution XPS spectra for Ti 2p (Figure 12b) and O 1s (Figure 12c) showed that both the before and after 20 cycles, samples exhibited the same species of Ti (Ti^{4+} and Ti^{3+}) and O (Ti-OH, Ti-O, Ti-O-P, and Ag-O). Additionally, as seen in Figure 12d,e, the composition of Ag species (Ag^0 and Ag^+) and P (P^{5+} in Ag_3PO_4) remained consistent in samples both before and after the 20th cycle. These results collectively confirmed the robust stability of R-PAgT-10:1, allowing it to maintain a stable performance during long-term H_2 evolution.

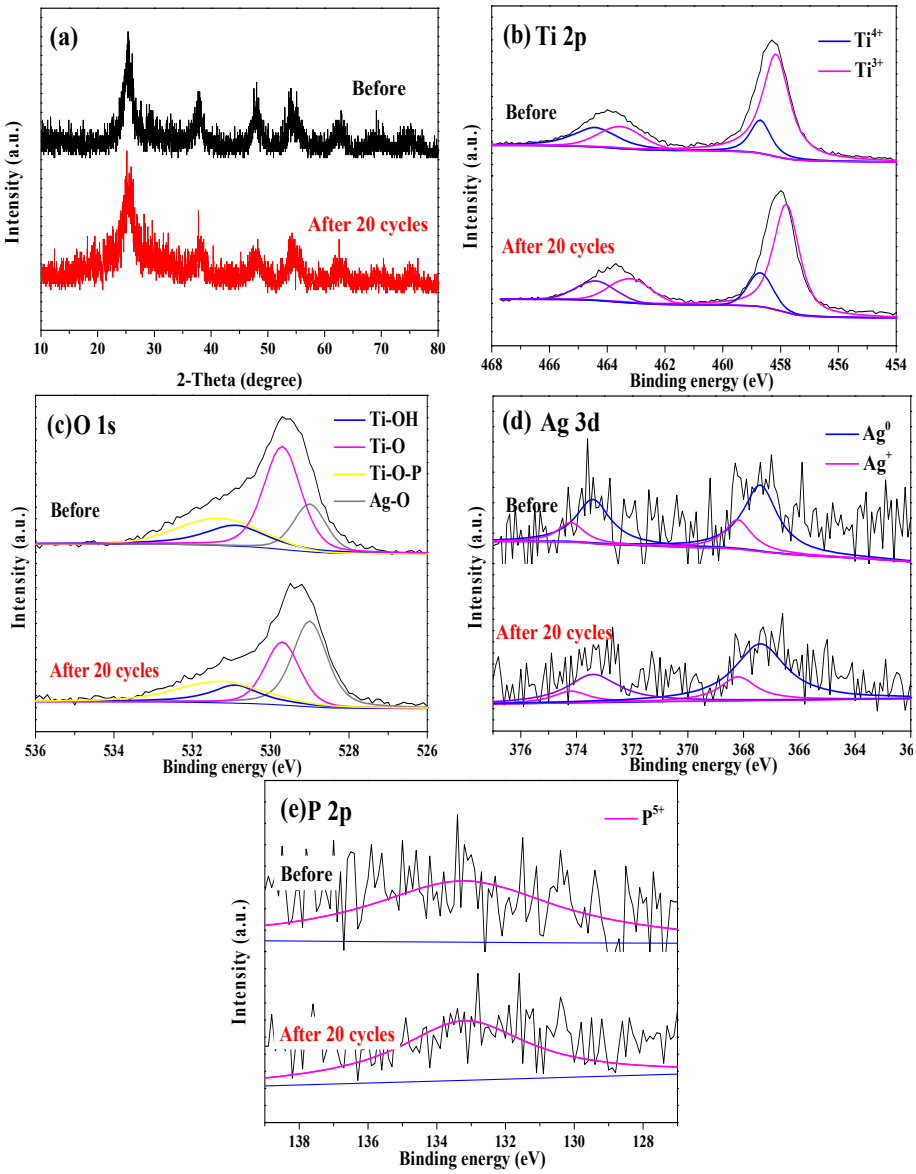

Figure 12. (**a**) XRD patterns, (**b**) Ti 2p, (**c**) Ag 3d, (**d**) O 1s, and (**e**) high-resolution P 2p XPS before and after the 20th cycle for R-PAgT-10:1.

3. Materials and Methods

3.1. Materials

Tetrabutyl titanate ($Ti(OC_4H_9)_4$, Wako 1st grade, ≥95.0% purity), silver nitrate ($AgNO_3$, guaranteed reagent, ≥99.5% purity), and silver phosphate (Ag_3PO_4, ≥99% purity) were sourced from FUJIFILM Wako Pure Chemical Industries, Ltd., Ibaraki, Japan. Additionally, ethanol (99.5% purity) from Kishida Chemical Co., Ltd. (Osaka, Japan) was employed as the solvent in the hydrothermal process. HNO_3 (1M) was used for dissolving the silver species. Sodium borohydride ($NaBH_4$, Wako 1st grade, ≥95.0% purity) served as the reducing agent. Methanol (≥99.7% purity), also obtained from FUJIFILM Wako Pure Chemical Industries, Ltd., Japan, was utilized as a sacrificial agent in the hydrogen evolution reaction. Deionized water was produced using the Milli-Q® water purification system (Merck, Rahway, NJ, USA).

3.2. Synthesis of the PAgT Photocatalyst

By using a hydrothermal method, the PAgT photocatalyst was synthesized [9]. In a typical procedure, Solution A was obtained by dissolving $Ti(OC_4H_9)_4$ (6 mL) into ethanol (46 mL) after stirring magnetically for 20 min. Subsequently, solution B was prepared, which consisted of 11 mL of $AgNO_3$, Ag_3PO_4, and HNO_3 (1M). Solution B was then slowly added dropwise to solution A with stirring vigorously to prepared solution C. The molar ratio of Ti to Ag was maintained at 10:1. Following continuous stirring for an additional 16 h; the solution C was transferred to a Teflon-lined autoclave (100 mL). After heating at 120 °C for 3 h and cooling down to room temperature, the pure PAgT photocatalyst was obtained and stored in the absence of light for subsequent steps.

3.3. Preparation of R-PAgT Composite with Different Mass Ratios of PAgT to $NaBH_4$

The OV-modified PAgT composite photocatalyst was prepared through the chemical reduction method using NaBH4 as reducing regent. The as-prepared PAgT (0.15 g) was well mixed with a certain amount of NaBH4. To clearly identify the reduced PAgT composites, the resulting products were designated as R-PAgT-X, where X represents the mass ratio of PAgT to $NaBH_4$. Specifically, the actual mass of $NaBH_4$ added for each ratio was as follows: 0.05 g for 3:1, 0.03 g for 5:1, 0.021 g for 7:1, 0.015 g for 10:1, and 0.01 g for 15:1. This systematic variation in $NaBH_4$ content allowed us to investigate its influence on the structural and chemical properties of the R-PAgT composites. Thereafter, the mixture was subjected to calcination in a tube furnace under a nitrogen atmosphere at 300 °C for 2 h, with a heating rate of 10 °C per minute. After cooling to room temperature, the obtained photocatalyst was washed with deionized water three times. Finally, the reduced PAgT powder was collected via centrifugation and was dried.

3.4. Characterizations

The crystal structure of R-PAgT was detected by XRD patterns by Rigaku Altima III Rint-2000 X-ray diffractometer with Cu Kα radiation range of 20–80°. The chemical composition of R-PAgT was measured through FT-IR (FT-IR-6800 JASCO instrument, JASCO Corporation, Tokyo, Japan) and XPS (JPS-9010MC photoelectron spectrometer, JEOL, Tokyo, Japan).

3.5. H_2 Evolution Experiment

The photocatalytic efficiency of the prepared R-PAgT photocatalysts for hydrogen (H_2) evolution was assessed using a closed, custom-built gas system. To simulate solar light, we employed a light source in the wavelength range of 300–780 nm (XC-100; SERIC. Ltd., Koshigaya, Saitama, Japan) positioned at a distance of 5 cm from the experimental setup. In each experimental run, the mixed solution of 7.5 mL methanol and 142.5 mL deionized water was the reaction medium. The dosage of PAgT and R-PAgT catalysts was 1 g/L. Prior to initiating the reaction, nitrogen gas was used to thoroughly replace the air in the system. Then, the system was exposed to simulated solar light (300–780 nm XC-100; SERIC., Ltd.) with an irradiance of 500 W/m^2 for a duration of 3 h. Following the irradiation, the H_2 gas generated during the reaction was collected at 30 min intervals and subsequently analyzed using a gas chromatography system (GC-8A; SHIMAZU, Tokyo, Japan). The gas chromatography system was equipped with a thermal conductivity detector and a Porapak Q column for the accurate detection and quantification of the produced H_2.

To assess the practical stability of R-PAgT, a series of ten consecutive cycles of H_2 generation experiments were carried out. As for the initial cycle, the procedure mirrored that of the individual experiment previously described. However, starting from the second round, the gaseous products generated in the preceding cycle were purged from the system using nitrogen (N_2) gas without introducing any new catalysts or methanol. This

sequence of steps was then repeated for a total of ten cycles to evaluate the sustained performance and stability of R-PAgT.

4. Conclusions

In this research, the OV-modified P/Ag/Ag_2O/Ag_3PO_4/TiO_2 composite photocatalyst (R-PAgT) was prepared through the chemical reduction method using $NaBH_4$ as the reducing regent. The findings provided critical insights into the impact of varying mass ratios of PAgT to $NaBH_4$ on the performance and stability of the photocatalyst. The optimized composite, R-PAgT-10:1, achieved a significantly enhanced H_2 evolution rate compared to the pure PAgT. This improvement was attributed to the moderate introduction of OVs, which effectively enhanced light absorption and charge separation. However, a higher mass ratio of PAgT to $NaBH_4$, specifically in the cases of R-PAgT-5:1 and R-PAgT-3:1, led to excessive OVs and the destruction of the crystal structure. These adverse effects resulted in diminished stability and reduced photocatalytic performance. Furthermore, R-PAgT-10:1 demonstrated remarkable stability, maintaining its enhanced H_2 evolution rate over 20 cycles under visible light irradiation. In conclusion, our study highlighted the significance of introducing OVs into the PAgT composite to enhance its H_2 evolution efficiency under intense solar light irradiation. Furthermore, the appropriate mass ratio of PAgT to $NaBH_4$ can induce a moderate amount of OVs, which is beneficial for achieving superior and stable H_2 evolution. These findings hold promise for the development of efficient and robust photocatalysts for renewable energy applications.

Supplementary Materials: The following supporting information can be downloaded at: www.mdpi.com/10.3390/catal15020167/s1, Figure S1: Schematic diagram of H2 evolution mechanism of PAgT under simulated solar light (adapted from (Sun et al., 2023 [28])). Table S1: Comparative photocatalytic H2 evolution rate over various OVs modified TiO2 photocatalysts (adapted from (Sun et al., 2023 [28])) [12,20,25–30].

Author Contributions: Writing—original draft preparation, X.S.; formal analysis, X.S., Y.Z., and G.A.; investigation, X.S., Y.Z., and G.A.; supervision, G.C. and Y.Y.; project administration, G.C. and Y.Y.; funding acquisition, Y.Y. All authors have read and agreed to the published version of the manuscript.

Funding: This research was supported by Scientific Research (B) 22H03778 and a Grant-in-Aid for Exploratory Research 21k19628 from the Japan Society for the Promotion of Science.

Data Availability Statement: Data will be made available on request by contacting the corresponding author.

Conflicts of Interest: The authors declare no conflicts of interest.

References

1. Huiqin, W.; Haopeng, J.; Pengwei, H.; Miroslave, E.; Libor, C.; Kamila, K. Hydrogen production from methanol-water mixture over NiO/TiO_2 nanorods structure photocatalysts. *J. Environ. Chem. Eng.* **2022**, *10*, 106908.
2. Subhasish, M.; Lopamudra, A.; Sharmila, S.; Kali, S.; Rashmi, A. Designing g-C_3N_4/$NiFe_2O_4$ S-scheme heterojunctions for efficient photocatalytic degradation of Rhodamine B and tetracycline hydrochloride. *Appl. Surf. Sci. Adv.* **2024**, *24*, 100647.
3. Bocheng, Q.; Lejuan, C.; Ning, Z.; Xiaoming, T.; Yang, C. A ternary dumbbell structure with spatially separated catalytic sites for photocatalytic overall water splitting. *Adv. Sci.* **2020**, *7*, 1903568.
4. Akira, F.; Kenichi, H. Electrochemical photolysis of water at a semiconductor electrode. *Nature* **1972**, *238*, 37–38.
5. Roberto, F.; Marianna, B.; Salvatore, S.; Leonardo, P. Photocatalytic H_2 production over inverse opal TiO_2 catalysis. *Catal. Today* **2019**, *312*, 113–119.
6. Devipriya, G.; Ashutosh, N.; Animes, G.; Nageswara, P. Ag-doped TiO_2 photocatalysts with effective charge transfer for highly efficient hydrogen production through water splitting. *Int. J. Hydrogen Energy* **2020**, *45*, 2729–2744.

7. Meng, S.; Min, W.; Qiang, W.; Jianjian, T.; Lingxia. Z.; Lianzhou, W.; Jianlin. S. A Ti-OH bond breaking route for creating oxygen vacancy in titania towards efficient CO_2 photoreduction. *Chem. Eng. J.* **2021**, *425*, 131513.
8. Rashmi, A.; Kulamani, P. A review on TiO_2/g-C_3N_4 visible-light- responsive photocatalysts for sustainable energy generation and environmental remediation. *J. Env. Chem. Eng*. **2020**, *8*, 103896.
9. Qi, Z.; Na, L.; Qiansu, M.; Aditya, S.; Daichi, N.; Xiang, S.; Cheng, Z.; Yingnan, Y. Sol-gel/hydrothermal two-step synthesis strategy for promoting Ag species–modified TiO_2-based composite activity toward H_2 evolution under solar light. *Mater. Today Energy* **2021**, *20*, 100648.
10. Bad'ura, Z.; Naldoni, A.; Qin, S.; Bakandritsos, A.; Kment, S.; Schmuki, P.; Zoppellaro, G. Light-Induced Migration of Spin Defects in TiO_2 Nanosystems and their Contribution to the H_2 Evolution Catalysis from Water. *ChemSusChem* **2021**, *14*, 4408–4414.
11. Xu, Z.Y.; Guo, C.Y.; Liu, X.; Li, L.; Wang, L.; Xu, H.L.; Zhang, D.K.; Li, C.H.; Li, Q.; Wang, W.T. Ag nanoparticles anchored organic/inorganic Z-scheme 3DOMM-TiO_2–based heterojunction for efficient photocatalytic and photoelectrochemical water splitting. *Chinese J. Catal.* **2022**, *43*, 1360–1370.
12. Wajid, S.; Yunqing, Z.; Xiaoyun, F.; Jie, Z.; Yingxuan, L.; Sumreen, A.; Chuanyi, W. Facile synthesis of defective TiO_{2-x} nanocrystals with high surface area and tailoring bandgap for visible-light photocatalysis. *Sci. Rep.* **2015**, *5*, 15804.
13. Rong, H.; Xiaoman, L.; Wangguo, G.; Xu, Z.; Sen, L.; Min, L. Recent advances in photocatalytic nitrogen fixation: From active sites to ammonia quantification methods. *RSC Adv.* **2021**, *11*, 14844–14861.
14. Dessy, A.; Laura, M.; Junzhe, D.; Yao, Y.; Wei, G. $NaBH_4$ modified TiO_2: Defect site enhancement related to its photocatalytic activity. *Mater. Chem. Phys.* **2017**, *199*, 571–576.
15. Zhao, Y.; Zhao, Y.; Shi, R.; Wang, B.; Waterhouse, G.I.N.; Wu, L.; Tung, C.; Zhang, T. Tuning oxygen vacancies in ultrathin TiO_2 nanosheets to boost photocatalytic nitrogen fixation up to 700 nm. *Adv. Mater.* **2019**, *31*, 1806482.
16. Andrea, L.; Patricia, R.; Carokina, G.; Rodrigo, S.; Patricio, V.; Paula, Z.; Pedro, O. FTIR and Raman characterization of TiO_2 nanoparticles coated with polyethylene glycol as carrier for 2-Methoxyestradiol. *Appl. Sci.* **2017**, *7*, 49.
17. Tobaldi, D.; Pullar, R.; Škapin, A.; Seabra, M.; Labrincha, J. Visible light activated photocatalytic behavior of rare earth modified commercial TiO_2. *Mater. Res. Bull.* **2014**, *50*, 183–190.
18. Xiaobo, Z.; Hanmin, T.; Xiangyan, W.; Guogong, X.; Zhipeng, T.; Jiyuan, Z.; Shikui, Y.; Tao, Y.; Zhigang, Z. The role of oxygen vacancy-Ti^{3+} states on TiO_2 nanotubes' surface in dye-sensitized solar cells. *Mater. Letters* **2013**, *100*, 51–53.
19. Hayat, K.; Zhuoran, J.; Dimitrios, B. Molybdenum doped graphene/TiO_2 hybrid photocatalyst for UV/visible photocatalytic applications. *Solar Energy* **2018**, *162*, 420–430.
20. Xudong, J.; Yupeng, Z.; Jing, J.; Yongsen, R.; Yancheng, W.; Yichu, W.; Chuxu, P. Characterization of oxygen vacancy associates within hydrogenated TiO_2: A Positron Annihilation Study. *J. Phy. Chem. C* **2012**, *116*, 22619–22624.
21. Xiaohu, H.; Qi, Z.; Xinlong, W.; Naoki, K.; Yingnan, Y. Nonmetal–metal–semiconductor-promoted P/Ag/Ag_2O/Ag_3PO_4/TiO_2 photocatalyst with superior photocatalytic activity and stability. *J. Mater. Chem. A* **2015**, *3*, 17858–17865.
22. Na, L.; Jie, M.; Aditya, S.; Xiang, S.; Naoki, K.; Guoping, C.; Yingnan, Y. Sustainable photocatalytic disinfection of four representative pathogenic bacteria isolated from real water environment by immobilized TiO_2-based composite and its mechanism. *Chem. Eng. J.* **2021**, *42*, 6131217.
23. Yang, G.; Tao, W. Preparation of Ag_2O/TiO_2 nanocomposites by two-step method and study of its degradation of RHB. *J. Mol. Struct.* **2021**, *1224*, 129049
24. Desong, W.; Lei, L.; Qingzhi, L.; Jing, A.; Xueyan, L.; Rong, Y.; Mangmang, Z. Enhanced visible-light photocatalytic performances of Ag_3PO_4 surface-modified with small amounts of TiO_2 and Ag. *Appl. Sur. Sci*. **2014**, *321*, 439–446.
25. Jingjing L., XuanLiang F, Shenfang C., Yongfa Z., Electronic structure and optical properties of Ag_3PO_4 photocatalyst calculated by hybrid density functional method, *Appl. Phys. Lett*. **2011**, *99*, 191903.
26. Xiaohong H., Qiansu M., Xinlong W., Yingjun Y., Na L., Cheng Z., Naoki K., Guoping C., Yingnan Y., Layered Ag/Ag_2O/$BiPO_4$/Bi_2WO_6 heterostructures by two-step method for enhanced photocatalysis, *J. Catal.* **2020**, *387*, 28-38.
27. Renquan G., Hongju Z., Jiaxin L., Yunfeng Q., Mingxin L., Muyao S., Zhao Z., Junkai Z., Dandan W., Huaqiao T., Reduced mesoporous TiO_2 with Cu_2S heterojunction and enhanced hydrogen production without noble metal cocatalyst, *Appl. Surf. Sci.* **2020**, *507*, 144772.
28. Sun, X.; Ming, J.; Ma, Q.; Zhang, C.; Zhu, Y.; An, G.; Chen, G.; Yang, Y. Fabrication of optimal oxygen vacancy amount in P/Ag/Ag_2O/Ag_3PO_4/TiO_2 through a green photoreduction process for sustainable H_2 evolution under solar light. *J. Colloid. Interf. Sci.* **2023**, *645*, 176–187.

29. Yajun Z., Zhongfei X., Guiyu L., Xiaojuan H., Weichang H., Yingpu B., Direct Observation of Oxygen Vacancy Self-Healing on TiO_2 Photocatalysts for Solar Water Splitting, *Angewandte Chemie* **2019**, *58*, 14229-14233.
30. Chia-Fen L., Tsong-Pyng P., Fabrication and band structure of Ag_3PO_4–TiO_2 heterojunction with enhanced photocatalytic hydrogen evolution, *Int. J. Hydrogen Energ*. **2020**, *45*, 149-159.